The Astrophysical Journal, 946:17 (10pp), 2023 March 20 https://doi.org/10.3847/1538-4357/acb143

Energetics of Shock-triggered Supersubstorms (SML < -2500 nT)

Bruce T. Tsurutani[1], and Rajkumar Hajra[2]
[1] Retired, Pasadena, CA, USA; bruce.tsurutani@gmail.com
[2] Indian Institute of Technology Indore, Simrol, Indore 453552, India
Received 2022 September 29; revised 2023 January 4; accepted 2023 January 5; published 2023 March 22

Abstract

The solar wind energy input and dissipation in the magnetospheric–ionospheric systems of 17 supersubstorms (SSSs: SML < -2500 nT) triggered by interplanetary shocks during solar cycles 23 and 24 are studied in detail. The SSS events had durations ranging from ∼42 minutes to ∼6 hr, and SML intensities ranging from −2522 nT to −4143 nT. Shock compression greatly strengthens the upstream interplanetary magnetic field southward component (B_s), and thus, through magnetic reconnection at the Earth's dayside magnetopause, greatly enhances the solar wind energy input into the magnetosphere and ionosphere during the SSS events studied. The additional solar wind magnetic reconnection energy input supplements the ∼1.5 hr precursor (growth-phase) energy input and both supply the necessary energy for the high-intensity, long-duration SSS events. Some of the solar wind energy is immediately deposited in the magnetosphere/ionosphere system, and some is stored in the magnetosphere/magnetotail system. During the SSS events, the major part of the solar wind input energy is dissipated into Joule heating (∼30%), with substantially less energy dissipation in auroral precipitation (∼3%) and ring current energy (∼2%). The remainder of the solar wind energy input is probably lost down the magnetotail. It is found that during the SSS events, the dayside Joule heating is comparable to that of the nightside Joule heating, giving a picture of the global energy dissipation in the magnetospheric/ionospheric system, not simply a nightside-sector substorm effect. Several cases are shown where an SSS is the only substorm that occurs during a magnetic storm, essentially equating the two phenomena for these cases.

Unified Astronomy Thesaurus concepts: Space weather (2037); Interplanetary magnetic fields (824); Interplanetary shocks (829)

1. Introduction

It is well recognized that local midnight-sector substorms (Akasofu 1964) are often triggered by interplanetary shock impingements onto the magnetosphere (Heppner 1955; Schieldge & Siscoe 1970; Kawasaki et al. 1971; Burch 1972; Kokubun et al. 1977; Akasofu & Chao 1980; Chua et al. 2001; Zhou & Tsurutani 2001; Boudouridis et al. 2003; Tsurutani & Zhou 2003; Liou et al. 2004; Yue et al. 2010, 2011, 2016; Ma et al. 2019; Oliveira et al. 2021; Zong et al. 2021). Zhou & Tsurutani (2001), using Polar UV data (Torr et al. 1995), have shown that midnight-sector substorm onsets started within ∼2 minutes of the shock compression of the magnetosphere, and that the energy for shock-induced substorms could be provided by precursor interplanetary magnetic field (IMF) southward (B_s) components up to ∼1.5 hr prior to the shock arrival. The authors speculated that energy inputs for time spans longer than ∼1.5 hr prior to the shock arrival would be dissipated away. They suggested that these shock-triggered substorms would be ideal events to study in order to determine the nightside triggering mechanism, because of the almost exact knowledge of the onset times. Such studies have not yet been performed, however, to the best of our knowledge.

In parallel related research, it has been noted that gradual—sometimes hours-long—solar wind ram pressure increases are correlated with geomagnetic activity (Brittnacher et al. 2000; Zesta et al. 2000; Chua et al. 2001; Shue & Kamide 2001; Boudouridis et al. 2003; Zhou & Tsurutani 2004; Shue et al. 2005, 2009). Zesta et al. (2000) noted that a strong solar wind pressure pulse caused the strengthening and widening of the auroral electrojet (AE) at all local times for the 1997 January 10–11 event. Shue & Kamide (2001), studying the same event, noted that a positive relationship existed between the solar wind density and the AE intensity. Shue & Kamide (2001) found that when the IMF was southward-directed, the dominant effect occurred with the westward electrojet. Boudouridis et al. (2003) found that solar wind pressure pulses caused a widening of the auroral oval and a decrease in the polar cap size during southward IMF conditions. Zhou & Tsurutani (2004) noted that gradual solar wind ram pressure increases caused dawn and dusk auroras, suggesting a Kelvin–Helmholtz instability energy transfer (viscous interaction; Axford & Hines 1961; Tsurutani & Thorne 1982) mechanism. Shue et al. (2009) noted that solar wind density enhancements caused AE enhancements under conditions of energy storage in the magnetotail. When the stored energy was drained by a prior substorm, the nightside auroral power did not respond to a density enhancement.

Both forward shocks and gradual solar wind pressure pulses cause dayside auroras and related phenomena (Zhou & Tsurutani 1999; Brittnacher et al. 2000; Chua et al. 2001; Tsurutani & Zhou 2003; Zhou et al. 2003; Ma et al. 2022). Zhou & Tsurutani (1999) showed that as the interplanetary shock moved downtail, the dayside auroras moved from noon toward dawn and dusk, indicating that the solar wind ram energy compressing the magnetosphere was being absorbed and dissipated. The mechanism for the dayside auroras is believed to be a combination of Joule heating (JH), Alfvén wave damping, and energetic particle precipitation (Zhou et al. 2003). For the latter mechanism, the compression of the remnant outer zone ∼10–100 keV electrons and ions leads to

$T_{\perp}/T_{||} > 1$ anisotropies, with the growth of electromagnetic chorus and electromagnetic ion cyclotron (EMIC) waves, respectively (Kennel & Petschek 1966; Zhou & Tsurutani 1999; Yue et al. 2011; Ma et al. 2022). The simultaneous generation of both electromagnetic wave types has been observed in such solar wind situations (Remya et al. 2015; Tsurutani et al. 2016). The waves then cyclotron resonate with energetic particles, causing pitch-angle scattering and loss into the ionosphere, creating the auroras (Tsurutani & Lakhina 1997). Of course, for long-duration pressure pulses (Zhou & Tsurutani 2004), the Kelvin–Helmholtz mechanism may be operative as well.

Yue et al. (2011) have found that injections of oxygen ions comparable to proton densities into the inner magnetosphere can occur after shock impacts. In a further study, Yue et al. (2016) noted that the H^+, He^+, and O^+ fluxes were enhanced in both the parallel and perpendicular directions to the ambient magnetic field after two shock impact events. Yue et al. (2017) noted that after the shock impingement, chorus waves intensified in the postmidnight to the prenoon sector, while the plasmaspheric hiss decreased on the dayside and intensified during night (however, see the contrary findings in Tsurutani et al. 2019 and Ma et al. 2022). Ma et al. (2019) found that for shock-triggered substorms with SME $>$ 1000 nT (including both traditional substorms and supersubstorms), $E < 200$ keV electron fluxes increased significantly. At the same time, $>$200 keV electron fluxes decreased. Oliveira et al. (2021) have shown that head-on shocks onto the dayside magnetosphere cause substorm energetic particle injections on the nightside that are more intense.

In a somewhat overlooked older paper, Nishida (1968) discussed the difference between DP1 (disturbance polar) current systems, which originate from the excitation of AEs or polar substorms, and DP2 current systems, which are counterparts of the convective system generated in the global magnetosphere. Further information about this will be given later in the paper, when discussing JH.

Recent attention has been focused on substorms with extreme intensities, which are called supersubstorms (SSSs; defined as SML < -2500 nT; Tsurutani et al. 2015). The SSS events have often been triggered by interplanetary shocks and high-density events (Tsurutani et al. 2015; Hajra et al. 2016). Hajra et al. (2016) showed that all SSS events studied from 1981 to 2012 were associated with strong IMF B_s fields. The reasoning behind the creation of such a new classification was that SSSs not only seemed to have intensities and durations that were much greater than those of a typical substorm, but their morphology also seemed to be different as well. It was also expected that such extreme events may be correlated with geomagnetically induced currents (GICs) on the ground, perhaps as a source of power outages. The former speculation was borne out by Hajra & Tsurutani (2018), who showed two SSS cases that did not have the standard midnight onset and following expansion. At the time of the SML index peak, the midnight sector was generally devoid of intense auroras, while the most intense auroras were located in the premidnight and postmidnight magnetic local times (MLTs). The latter suggestion was substantiated by Tsurutani & Hajra (2021), who showed that GICs at the Mäntsälä Finland pipeline were indeed associated with SSS events. Although Tsurutani & Hajra (2021) and Hajra (2022a, 2022b) have shown that strong GICs at Mäntsälä Finland were associated with shock-induced SSS events, a question still remains: what is it about SSS events that cause GICs? This is not understood at the present time. The Zong et al. (2021) paper on shock-triggered SSS events (defined as SME $>$ 2000 nT) and shock-triggered substorms with SME $>$ 1000 nT gives an excellent review of SSS events.

More recently, Despirak et al. (2020a), in a case contrary to that of Hajra & Tsurutani (2018), found SSS events that were characterized by strong nightside disturbances as well as the simultaneous development of dayside magnetic bays at polar latitudes. Those authors speculated that the westward ionospheric current shifted to the dayside. Despirak et al. (2020b) studied five SSS events (defined as SML < -2000 nT) in 2012 and 2017 (see also Despirak et al. 2019a), and found that for the two SSS events with SML < -2500 nT, "strong jumps in the density and ram pressure" and "high B_s values" preceded them. These two interplanetary events are expected to be fast-forward shocks, but this has not yet been verified. Despirak et al. (2020c) showed that two SSS events on 2001 April 11–12 were associated with high densities in the interplanetary sheath downstream of a shock. Despirak et al. (2021) identified an SSS event (SML < -2500 nT) that occurred inside a magnetic cloud (MC) where there was no obvious density trigger. However, there was a sharp IMF B_y switch prior to the event. The MC B_z component at the time was deeply southward. Despirak et al. (2019b) have performed a statistical survey of SSS events between 1998 and 2016. They find that most events occur during magnetic storms with a small percentage in geomagnetic quiet. These results are similar to those of Hajra et al. (2016), who did a statistical study of SSS events from 1981 to 2012.

Although there are still many unknowns in relation to SSS events, the purpose of this paper is to focus on one of the principal outlying problems—the source of the energy for shock-triggered substorm events. Zhou & Tsurutani (2001) have shown that a precursor IMF $B_s \sim 1.5$ hr prior to the shock arrival could supply the necessary energy for a shock-triggered lower-intensity substorm. However, when SSS events were later examined, Hajra & Tsurutani (2018) noted in several cases that there was insufficient precursor energy to explain some of the SSS events that were studied. It was therefore concluded that some other source of energy must supplement the precursor energy input. To resolve the issue of the source of the energy for shock-triggered SSS events, we will study the solar wind input energy and the energy dissipations of all the SSS events that were triggered by interplanetary shocks between 1997 and 2021 (solar cycles 23 and 24). We will also focus on why SSSs are unusually intense and long-lasting (often $\sim$3 hr duration).

2. Database and Analyses

The SSS events examined in this study are defined as having a SuperMAG westward AE index SML minimum <-2500 nT (Tsurutani et al. 2015). The 1 minute SML index data are collected from the SuperMAG site (Gjerloev 2012).[3] From the temporal variations of the SML indices, sharp decreases in SML, leading to negative bay developments, are identified as substorms (Rostoker et al. 1980; Newell & Gjerloev 2011). A list of all the substorms with SML peaks <-2500 nT (SSS events) from 1981 to 2012 has been developed by Hajra et al. (2016). We have updated the list to include recent events from

[3] https://supermag.jhuapl.edu/

2012 to 2021. For the present study, we have only selected the interplanetary shock-triggered SSS events occurring between 1997 and 2021, or events in solar cycles 23 and 24. The high–time resolution interplanetary data necessary for detailed shock analyses prior to 1997 were often quite sparse, so it was not possible to extend the study interval earlier in time, in a meaningful way. Along with the SML indices, based on observations at approximately 110 stations, dayside and nightside SML indices are also shown in this work. They are derived from stations that are located under the sunlit ionosphere and under the dark ionosphere, respectively.

The SSS energy budget is studied by estimating the energy transfer from the solar wind to the magnetosphere, and the dissipation of the energy in the inner magnetosphere–ionosphere system (e.g., Turner et al. 2006, 2009; Guo et al. 2011, 2012; Hajra et al. 2014; Verkhoglyadova et al. 2016). As no direct measurement of the solar wind input energy rate is available, we use the Perreault & Akasofu (1978) ε-parameter ($V_{sw}B_0^2\sin^4(\theta/2)R_{CF}^2$), based on a consideration of the magnetic reconnection during southward IMFs, leading to solar wind energy transfer to the magnetosphere. In the ε-expression, V_{sw} is the speed of the solar wind plasma, B_0 is the IMF magnitude, θ is the clock angle between the geomagnetic field vector and the IMF vector in the equatorial plane, and R_{CF} is the magnetosphere scale size, which varies depending on the solar wind conditions (Chapman & Ferraro 1931; Monreal-MacMahon & Gonzalez 1997; Shue & Chao 2013).

The solar wind energy is dissipated in the magnetosphere in the form of ring current (RC) energy, in the auroral ionosphere, as JH, and as auroral-zone energetic particle precipitation (AP). The RC energy dissipation rate is estimated as $d\text{SYM-H}^*/dt + \text{SYM-H}^*/\tau$ (Akasofu 1981), where SYM-H* is the solar wind pressure-corrected SYM-H index (Burton et al. 1975; Gonzalez et al. 1989; Turner et al. 2001) and τ is the average RC decay time, taken as 8 hr for the present study (Yokoyama & Kamide 1997; Guo et al. 2011). The JH rate is calculated according to $a|\text{PC}| + b\text{PC}^2 + c|\text{SYM-H}| + d\text{SYM-H}^2$ (Knipp et al. 2004), where PC is the polar cap potential index and a, b, c, and d are season-dependent parameters. The AP rate data are obtained from the National Oceanic and Atmospheric Administration (NOAA)/Television Infrared Observation Satellite (TIROS) measurements[4] of high-latitude precipitating ∼50 eV–20 keV electron and ion fluxes (Foster et al. 1986; Fuller-Rowell & Evans 1987; Emery et al. 2006).

From the above energy rates/powers, the total solar wind energy input and the magnetospheric/ionospheric dissipation energies are calculated by integrating the power terms during the SSS growth phases (McPherron 1970) as well as during the entire SSS intervals, from the beginnings of the growth phases to the ends of the recovery phases. Because the prior work of Zhou & Tsurutani (2001) indicated that the growth-phase energy was only stored ∼1.5 hr prior to substorm onset, we have also calculated the total solar wind input to the magnetosphere, from 1.5 hr prior to the shock arrival to the end of the substorm recovery phase. Both estimations will be discussed later in the paper, in light of the total magnetospheric/ionospheric dissipation rates.

To identify a fast magnetosonic interplanetary shock, we calculate the interplanetary discontinuity normal vector and its angle (θ_{Bn}) relative to the upstream IMF. The normal direction is determined using the Abraham-Shrauner (1972) mixed-mode method. The Rankine–Hugoniot conservation equations (Rankine 1870; Hugoniot 1887, 1889) are applied to upstream and downstream plasmas and magnetic fields (Smith 1985; Tsurutani & Lin 1985; Tsurutani et al. 2011; Hajra et al. 2020). The magnetosonic Mach number (M_{ms}) is calculated by comparing the calculated discontinuity speed to the upstream magnetosonic wave speed. For the magnetosonic interplanetary shocks, $M_{ms} > 1$.

The 1 minute resolution solar wind plasma and IMF data analyzed in this work are obtained from the OMNI website.[5] The SYM-H index data (1 minute resolution) are obtained from the World Data Center for Geomagnetism, Kyoto, Japan.[6] Along with SYM-H, we also show symmetric RC indices based on available magnetometer stations (located between −50° and +50° magnetic latitudes) in four equally sized MLT sectors centered at 00 MLT, 06 MLT, 12 MLT, and 18 MLT. Thus, 00 MLT corresponds to all MLTs from 21 MLT to 03 MLT, and similar 6 hr intervals apply to the other time sectors. These MLT-dependent SYM-H indices are obtained from SuperMAG. Using these SYM-H values, we have also estimated the JH rates at the four MLT sectors, following the method described above.

3. Results

3.1. Case Studies

Figure 1 shows the solar wind properties and geomagnetic responses during the SSS event on day 218 of 1998, and the corresponding energy budget estimations. The vertical black dashed line shows the southward turning of the IMF at ∼01:00 UT on day 218 (Figure 1(d)), leading to the start of the substorm growth phase. The IMF B_z has an almost steady southward component of ∼−8 nT during the growth phase. The IMF turning southward causes the beginning of the solar wind energy input, as seen in the enhancement of the ε-parameter (Figure 1(e)). At the same time, there is a slow increase in the RC energy, JH, and AP dissipation rates (Figure 1(e)). The magnetosphere/magnetotail energy storage will occur in parallel with this, as hypothesized by Zhou & Tsurutani (2001). The energy dissipated in the substorm growth phase is presumably the cause of the limited amount of time (∼1.5 hr) for energy storage (Zhou & Tsurutani 2001).

The vertical solid red line at ∼07:41 UT marks the shock impingement onto the magnetosphere. At this time, there are abrupt increases in V_{sw} (∼372 to 431 km s^{-1}), N_{sw} (∼10 to 24 cm^{-3}), P_{sw} (∼3 to 8 nPa), T_{sw} (∼2×10^4 to 5×10^4 K), and IMF B_0 (∼10 to 19 nT). The jump conditions are consistent with a fast-mode shock. The calculated shock M_{ms} is ∼1.3, and the shock is found to propagate at θ_{Bn} of ∼77°, with respect to the ambient IMF. The shock causes a sharp rise in SYM-H from −21 to +3 nT (Figure 1(f)). This latter feature is a sudden impulse (SI$^+$).

The vertical solid red line also marks a sharp decrease in the SML index (Figure 1(g)), defining the substorm expansion phase onset. This is clearly a shock-triggered substorm event. The substorm SML attains a peak value of −2960 nT at 09:42 UT on day 218, and the substorm recovery starts after this. The SML index attains the presubstorm level of ∼−340 nT at

[4] https://www.ngdc.noaa.gov/stp/satellite/poes/dataaccess.html

[5] http://omniweb.gsfc.nasa.gov/

[6] https://wdc.kugi.kyoto-u.ac.jp/

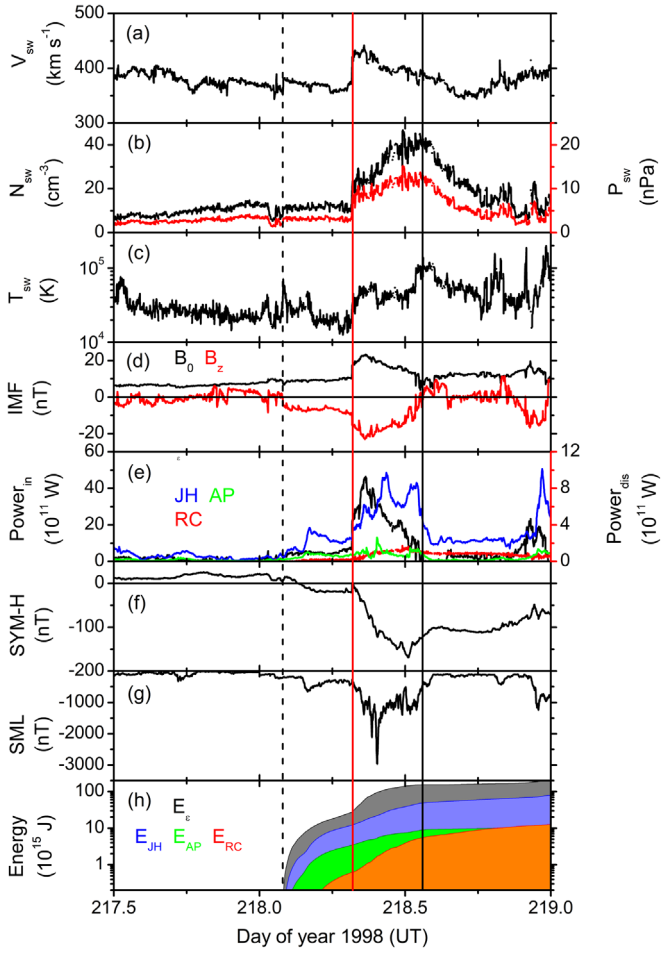

Figure 1. An SSS on day 218 of year 1998. From top to bottom, the panels show (a) the solar wind speed V_{sw}; (b) the plasma density N_{sw} (black; the legend to the left) and ram pressure P_{sw} (red; the legend to the right); (c) the temperature T_{sw}; (d) the IMF magnitude B_0 (black) and B_z component (red); (e) the solar wind energy input rate ε/"power" (black; the legend to the left), the energy dissipation rates through JH (blue; the legend to the right), AP (green; the legend to the right), and the RC energization rate (red; the legend to the right); (f) the symmetric RC index SYM-H; (g) the westward AE index SML; and (h) the integrated ε energy (black) input and the integrated JH (blue), AP (green), and RC (red) energy dissipations. The vertical black dashed line indicates the southward turning of the IMF, marking the beginning of the substorm growth phase. The solid red line shows both the shock impingement time onto the magnetosphere and the onset of the SSS expansion phase, as indicated by the sharp decrease in the SML index. The solid black line indicates the end of the substorm recovery phase.

~13:31 UT on day 218. This is marked by a vertical black line indicating the end of the substorm recovery phase. The duration of the SSS, from the expansion phase onset to the end of the substorm (excluding the growth phase), was ~5 hr and 50 minutes. The duration and intensity of this shock-triggered SSS event are extraordinary. The Akasofu (1964) scenario of an ionospheric substorm may not pertain to events like these (see Hajra & Tsurutani 2018).

The ε-parameter attained its peak value (~46×10^{11} W) in the SSS expansion phase (at ~08:45 UT on day 218), while the dissipation rates for JH, AP, and RC energy attained their peak values (~9.7×10^{11}, 2.6×10^{11}, and 1.7×10^{11} W, respectively) at or after the SSS peak value (at ~10:27, 09:42, and 11:46 UT on day 218, respectively).

In the interplanetary sheath downstream of the shock, the southward IMF component is found to intensify from ~–8 nT to ~–23 nT (Figure 1(d)). The shock is compressing the upstream southward IMF, leading to the intensification of that component (see Tsurutani et al. 1988). The enhanced southward IMF leads to an increase in the solar wind input energy rate (ε). As a consequence, there are increases in the ionospheric JH, AP, and magnetospheric RC dissipation rates (Figure 1(e)), which are associated with the increased interplanetary sheath energy input.

From the variation of the SYM-H index, the SSS is found to occur in the main phase of an intense geomagnetic storm, with a SYM-H minimum value of −169 nT at ~12:17 UT (Figure 1(f)). There are no other major substorms other than the SSS event in the magnetic storm. The shock-triggered SSS event and the magnetic storm appear to be the same thing. This will be discussed in more detail later in the paper.

The integrated input and dissipation energies, from the substorm growth phase to the end of the recovery phase, are shown in Figure 1(h). The total magnetospheric energy input during the growth phase (before the SSS onset) is ~27×10^{15} J. After the SSS expansion phase onset, additional energy of ~126×10^{15} J is input up to the end of the substorm interval. Thus, larger amounts of energy are injected during the expansion and recovery phases of the SSS than during its growth phase. During the substorm interval (from the substorm expansion phase to the recovery phase), the total energy dissipated through JH is ~49×10^{15} J, that through AP is ~9×10^{15} J, and that through the RC energy is ~6×10^{15} J. The dissipation partitions of the total solar wind input energy (from the substorm growth phase to the recovery phase) are ~32% (JH), ~6% (AP), and ~4% (RC energy). It can be noted from the curves that the energy dissipated in the magnetosphere/ionospheric system (JH + RC+ AP) during the SSS expansion and recovery phases is larger than the precursor energy input during the growth phase.

It can be concluded that the continuous energy injection in the magnetosphere during the SSS is important, as well as the energy loading during the growth phase. The energy input for the full growth phase is ~27×10^{15} J and for the 1.5 hr growth phase it is ~9×10^{15} J. It is clear that neither of the precursor events are sufficient to supply the total SSS energy dissipation (~64×10^{15} J). It should also be noted that the major part of the SSS energy goes into JH, and that the AP and the RC energies are relatively small in comparison.

Figure 2 shows the local time–dependent JH energy during the SSS event in Figure 1. What is particularly interesting is that during the substorm growth phase (from the vertical dashed black line to the vertical solid red line), JH occurs equally at all local times (Figure 2(a)). After the SSS expansion phase onset (the vertical red line), the JH values at 12 MLT and 18 MLT (the noon to afternoon sector) are actually slightly higher than those at midnight (00 MLT) and dawn (06 MLT). This feature is present until the peak of the SSS event at 09:42 UT. Figures 2(d) and (e) show scatterplots of nightside JH with the dayside JH. Interestingly, linear variations are observed up to JH values of ~5×10^{11} W, beyond which there is large scattering. This may be associated with the slightly higher JH values for the noon to afternoon sector than for the midnight to dawn sector. However, the overall correlation coefficients ($r \geqslant 0.89$) are high, indicating the equivalence of the dayside and nightside JH. Although the SSS peak intensity appears as a sharp downward spike, this is not reflected in either the JH or RC energy. After the SSS peak, the JH is at its highest at 18

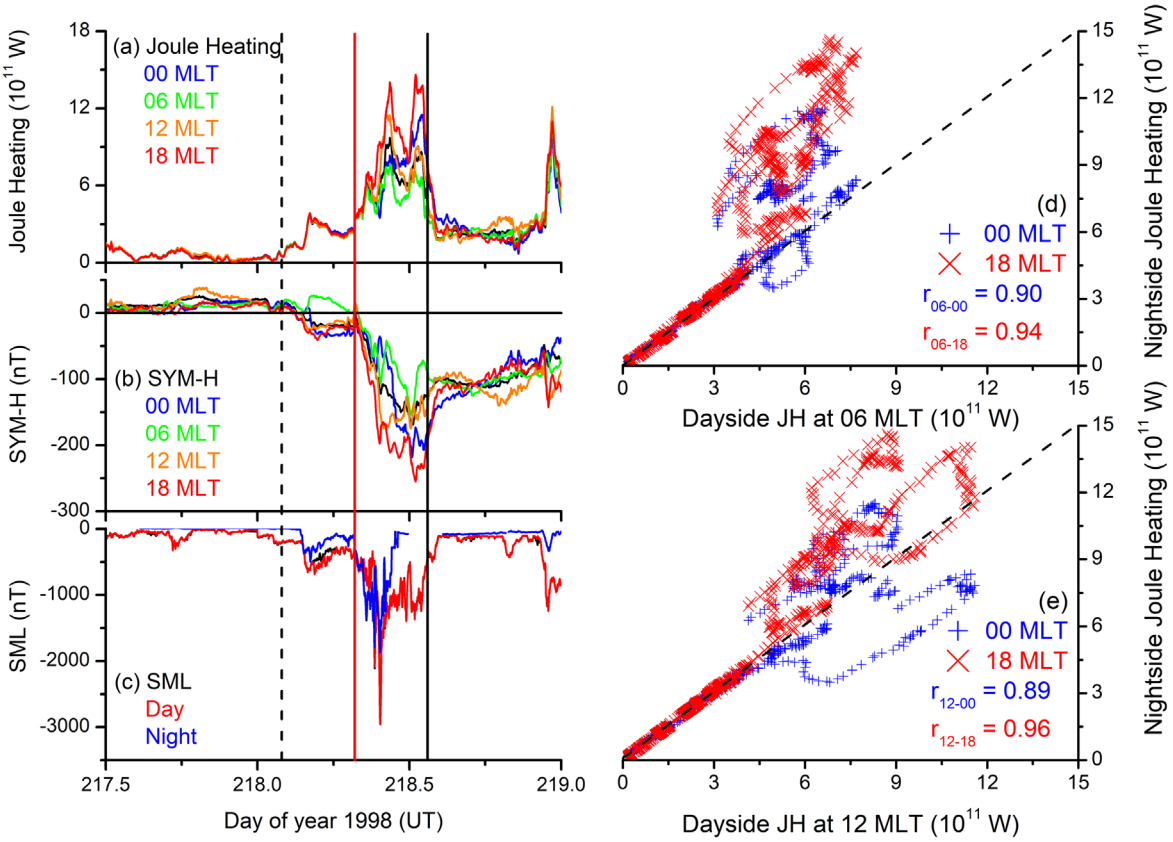

Figure 2. Left: temporal variations of (a) the overall JH rate (black) and the JH rates at 00 MLT (blue), 06 MLT (green), 12 MLT (orange), and 18 MLT (red); (b) the symmetric RC index SYM-H (black) and partial RC indices at 00 MLT (blue), 06 MLT (green), 12 MLT (orange), and 18 MLT (red); and (c) the westward AE index SML (black), the dayside SML (red), and the nightside SML (blue) during the SSS on day 218 of year 1998. The beginning of the substorm growth phase (the vertical black dashed line), the shock impingement onto the magnetosphere and the onset of the substorm expansion phase (the solid red line), and the termination of the substorm recovery phase (the solid black line) are marked as they were in Figure 1. Right: variations of the nightside JH at 00 MLT and 18 MLT, with (d) the dayside JH at 06 MLT and (e) the dayside JH at 12 MLT, during the SSS expansion to the recovery phases. The corresponding linear regression coefficients (r) are mentioned in the panels. Diagonal (dashed) lines are added to indicate equal values.

MLT. When the SML index is separated into dayside and nightside SML indices, the dayside SML values are generally found to be larger than the nightside SML values.

The SYM-H local time values indicate that during the long substorm growth phase, the local time sectors of 00, 12, and 18 MLT show essentially the same value, indicating the development of a symmetric RC during this phase of geomagnetic activity. After the onset of the SSS expansion phase, the 18 MLT sector SYM-H index is the most negative. This is consistent with the scenario of the substorm-injected energetic ions drifting from the midnight sector to dusk local times.

Figure 3 shows another example of an SSS that occurred on days 250–251 of 2017. The format is the same as for the previous case (Figure 1). The southward turning of the IMF started at ~20:30 UT on day 250 (Figure 3(d)), with the slow increase in the solar wind (ε) energy input (Figure 3(e)). The IMF B_z component is nearly steady at ~–10 nT during the interval of 2 hr and 31 minutes prior to the shock arrival.

The substorm growth phase is accompanied by slightly enhanced JH (Figure 3(e)) and a slow build up in RC (the decrease in SYM-H: Figure 3(f)). It is assumed that energy is being stored in the magnetosphere and magnetotail as well (Zhou & Tsurutani 2001).

An interplanetary fast-mode shock occurs at ~23:01 UT on day 250. The shock is characterized by a sharp increase in V_{sw} (~477 to 708 km s^{-1}), N_{sw} (~3 to 9 cm^{-3}), P_{sw} (~1 to 6 nPa), T_{sw} (~2×10^4 to 58×10^4 K), and IMF B_0 (~10 to 25 nT). This plasma and field discontinuity is a shock propagating at θ_{Bn} of ~48°, with respect to the ambient IMF. The calculated shock M_{ms} is ~3.1. The shock caused an SI$^+$ of +42 nT (Figure 3(f)). The shock compressed the upstream IMF B_z (−10 nT) to a value of ~−31 nT at ~23:23 UT. This is the same general phenomenon that occurred in the previous SSS event, shown in Figure 1: a shock compression of upstream southward-directed IMFs. The enhanced southward IMF in the interplanetary sheath causes an abrupt increase in the solar wind ε input energy. This increase in the energy injection is partially dissipated into JH, AP, and RC energy (Figure 3(e)). The SSS attained its peak intensity of −3712 nT at 00:24 UT on day 251. The SSS ended at ~01:25 UT (the vertical solid black line). The SSS expansion and recovery phases had a total duration of ~2 hr and 24 minutes.

During the substorm growth phase (between the vertical black dashed line and the solid red vertical line), the total solar wind energy input is ~16×10^{15} J. This is significantly less than the total energy input of ~186×10^{15} J, from the substorm expansion phase to the end of the substorm recovery. Thus, more energy is injected into the magnetosphere during the substorm expansion and recovery phases than in the growth phase. From the total solar wind input energy (~202×10^{15} J),

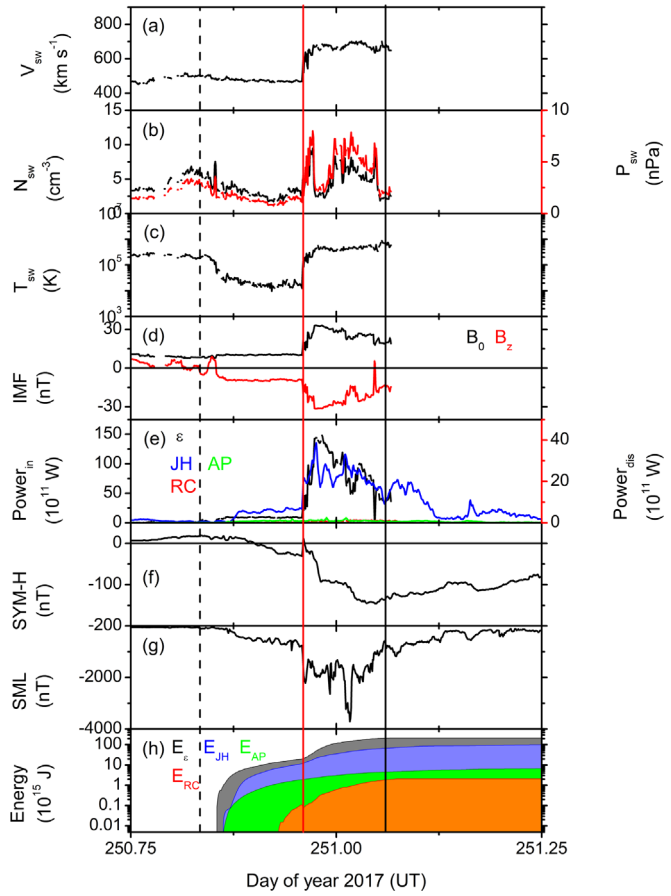

Figure 3. An SSS on days 250–251 of year 2017. The panels are in the same format as in Figure 1. The start of the substorm growth phase is indicated by the vertical dashed line, both the shock impingement onto the magnetosphere and the onset of the substorm expansion phase by the solid red line, and the end of the SSS event by the vertical black line.

only $\sim 66 \times 10^{15}$ J ($\sim$33%) is dissipated as JH, $\sim 5 \times 10^{15}$ J ($\sim$2%) as AP, and $\sim 2 \times 10^{15}$ J ($\sim$1%) as RC energy. Again, the dominant energy dissipation into the magnetosphere/ionosphere system is JH.

The SSS event (Figure 3(g)) is the only substorm that occurs during the magnetic storm (Figure 3(f)). The magnetic storm has a peak SYM-H value of −146 nT at ∼01:08 UT on day 251. It is noted that the SSS peak at ∼00:24 UT causes a decrease in the SYM-H index, from a value of −133 nT to −146 nT. The SSS event and the magnetic storm are closely related, if not the same thing.

During the substorm growth phase (between the vertical dashed line and the vertical solid red line), JH is essentially the same at all local times (Figure 4(a)). This is again confirmed by scatterplots of the nightside JH with the dayside JH, revealing a high correlation value ($r = 0.99$) between the two (Figures 4(d)–(e)). The RC energy gradually builds up, with the 12 MLT and 18 MLT sectors showing larger amounts of deposition than the 00 MLT and 06 MLT sectors (Figure 4(b)). The SML day and night indices are essentially the same (Figure 4(c)). An equal amount of JH energy is dissipated in the daytime as in the nighttime.

In the SSS expansion and recovery phases (between the vertical red line and the vertical black line), JH is equally present at all local times. The dayside and nightside SML indices are essentially equal.

3.2. Statistical Results

To assess the statistical significance of the results obtained from the case studies shown in Figures 1–4, we have performed a similar energy budget study for all the shock-initiated SSS events between 1997 and 2021 (solar cycles 23 and 24). The events and their energy budgets are listed in Table 1.

From Table 1, it can be noted that the peak SSS intensity ranged from −2522 nT to −4143 nT, with a mean value of −3021 nT. The durations of the substorm growth phases ranged from ∼28 minutes to ∼11 hr and 38 minutes, with a mean growth-phase duration of ∼3 hr and 17 minutes. The durations of the substorm expansion phases to the ends of the recovery phases ranged from ∼42 minutes to ∼5 hr and 51 minutes, with a mean SSS duration of ∼2 hr and 25 minutes. The SSS (phase) durations are consistent with the durations of the IMF southward components.

The solar wind energy input (ε) during the growth phase (before the onset of the SSS expansion phase) is less than the total SSS energy dissipation in nine of 17 cases (Table 1; the corresponding SML peak times are marked by the use of the bold font). If the Zhou & Tsurutani (2001) hypothesis, that the magnetosphere/magnetotail can only store energy for ∼1.5 hr prior to the onset of the substorm expansion phase, should be correct, then this number would be even less, with 12 of 17 cases (Table 1). The SSS JH accounts for ∼7%–84% (average ∼30%) of the solar wind input energy. AP accounts for 0%–10% (∼3%) and RC accounts for only ∼0%–4% (average ∼2%) of the solar wind input energy. On average, one-third of the total solar wind energy input is dissipated as the SSS energy, and the major part of this goes into JH. Quantitatively, ∼85% of the total SSS dissipation energy goes into JH, and only ∼9% and ∼6% of the SSS energy go into the AP and RC energy, respectively. It is probable that much of the solar wind energy (the other two-thirds of the ε energy input) goes down the tail and is not deposited as magnetospheric or ionospheric energy. The above numbers are in agreement with this general picture.

Figure 5 shows the variations of the dissipation energies with the solar wind energy input during the SSS growth phase (left) and from the SSS growth phase to the end of the SSS recovery phase (right). The corresponding regression lines, regression (correlation) coefficients (r), and statistical confidence levels (c) are noted in each panel.

It is interesting to note that there is no significant association of the SSS dissipation energies with the energy input during the growth phase. The correlation coefficient r varies between 0.22 and 0.45. However, the SSS dissipation increases linearly with the increasing input energy during the entire SSS interval. The correlation coefficient is significantly high, except for the AP. The strong association between the input and dissipation energies, as confirmed by the high r values, is indicative of a direct driving process occurring during the SSS events.

4. Summary and Discussion

The solar wind input energy and magnetospheric/ionospheric dissipation energy budgets during shock-induced SSS events have been determined for all 17 events occurring during solar cycles 23 and 24. The two solar wind precursor/substorm growth-phase (the full growth phase and the ∼1.5 hr growth phase) energies were considered separately. The durations of the SSS events lasted between ∼0.7 and ∼5.9 hr. The intensities of the SSS events ranged from −2522 nT to −4143 nT.

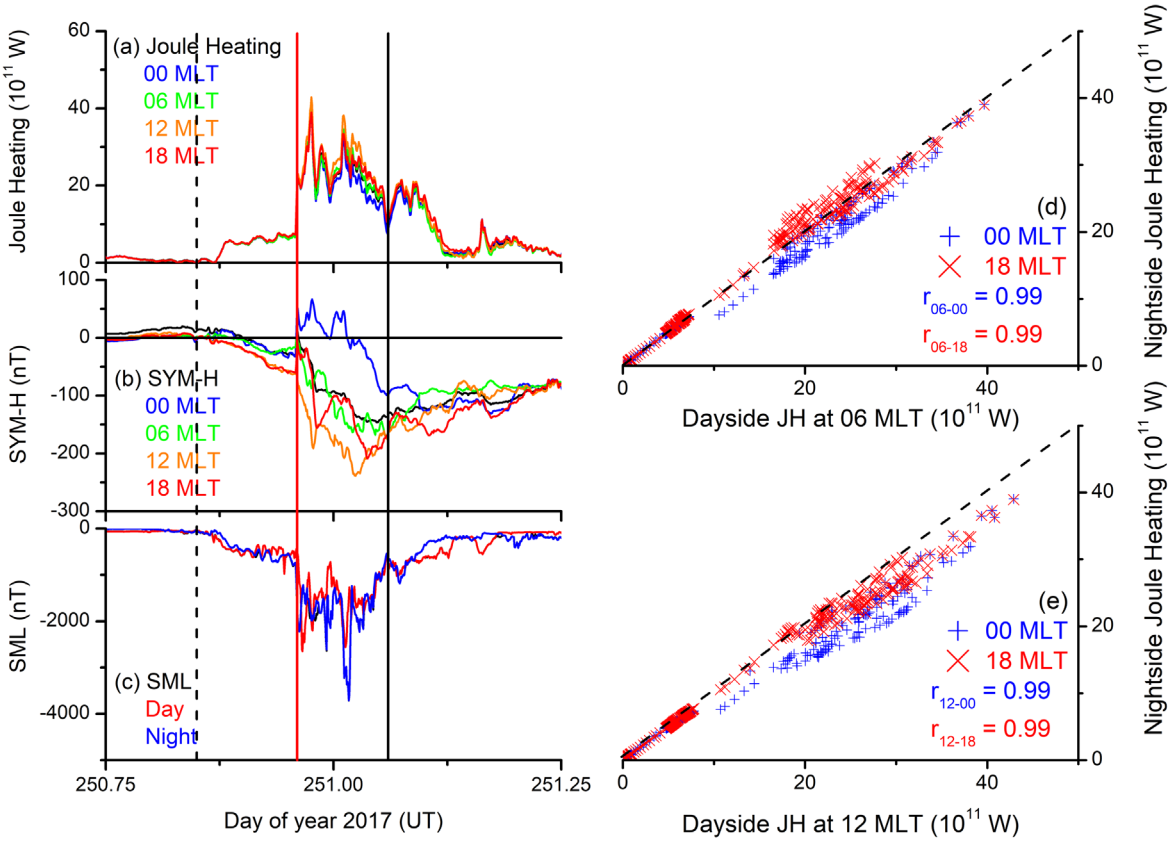

Figure 4. Left: variations of (a) the JH rate, (b) the symmetric RC index SYM-H, and (c) the westward AE index SML during the SSS on days 250–251 of year 2017. Right: variations of the nightside JH with (d) the dayside JH at 06 MLT and (e) the dayside JH at 12 MLT during the SSS expansion to the recovery-phase intervals. The panels are in the same format as in Figure 2. The vertical lines denote the same substorm-phase features as in Figure 3.

Table 1
SSS Energy Budget

SML Peak Time (Year Day UT)	SML Peak (nT)	SSS Duration (hr)		Energy Input (10^{15} J)		Energy Dissipation (10^{15} J)		
		Growth Phase	Expansion to Recovery	Growth Phase	Total	JH	AP	RC
1998 124 03:33	−2958	11.65	3.68	53.5 (8.6)[a]	468.7	85.8	13.9	8.2
1998 218 09:42	−2960	5.78	5.85	27.4 (9.1)[a]	153.8	49.1	8.9	5.5
1999 49 10:50	−2531	3.38	4.82	86.8 (34.5)[a]	321.4	50.1	7.7	4.0
2000 225 15:15	−2522	8.05	3.37	652.2 (74.6)[a]	793.5	111.6	10.2	14.1
2000 279 12:09	−2787	0.48	2.08	13.0	71.6	21.8	2.8	2.9
2001 101 16:09	−2923	1.13	0.77	18.0	69.3	10.3	2.2	0.3
2001 103 10:48	−2841	1.22	1.15	13.4	23.0	19.3	2.4	0.6
2001 328 07:07	−3839	0.82	0.72	76.0	200.1	139.0	3.2	0.5
2001 328 13:52	−3312	3.00	0.75	342.9 (55.3)[a]	381.9	71.7	4.2	4.7
2003 324 16:32	−3033	0.58	2.38	57.3	1785.9	302.9	3.8	20.3
2004 209 08:32	−2933	3.33	2.67	241.1 (119.4)[a]	490.4	59.5	8.9	6.7
2004 313 04:05	−2831	7.27	1.27	1338.9 (360.8)[a]	1614.7	239.8	8.1	11.3
2005 19 11:21	−2685	2.85	2.40	51.1 (23.4)[a]	93.1	63.6	7.2	2.7
2005 135 08:50	−2683	2.55	1.47	849.2 (478.9)[a]	1055.2	68.8	3.8	6.6
2005 236 10:18	−4143	0.50	2.28	82.6	469.6	36.0	4.6	2.0
2010 95 09:29	−2668	0.87	3.15	3.3	30.7	14.1	3.0	0.8
2017 251 00:24	−3712	2.50	2.42	16.1(8.5)[a]	201.7	66.4	4.6	1.8

Note.
[a] The values in parentheses show the energy inputs during a period of 1.5 hr prior to the expansion phase onset, for cases with longer-duration growth phases. The SML peak times for the cases with growth-phase energy inputs less than the total SSS energy dissipation are marked in bold font.

Of the total energy dissipated by the magnetospheric/ionospheric system during the SSS events, the great majority (∼85%) goes into JH. The AP and RC energy inputs account for only ∼9% and ∼6% of the SSS energy, respectively. These statistics are the averages for all 17 shock-triggered SSS events.

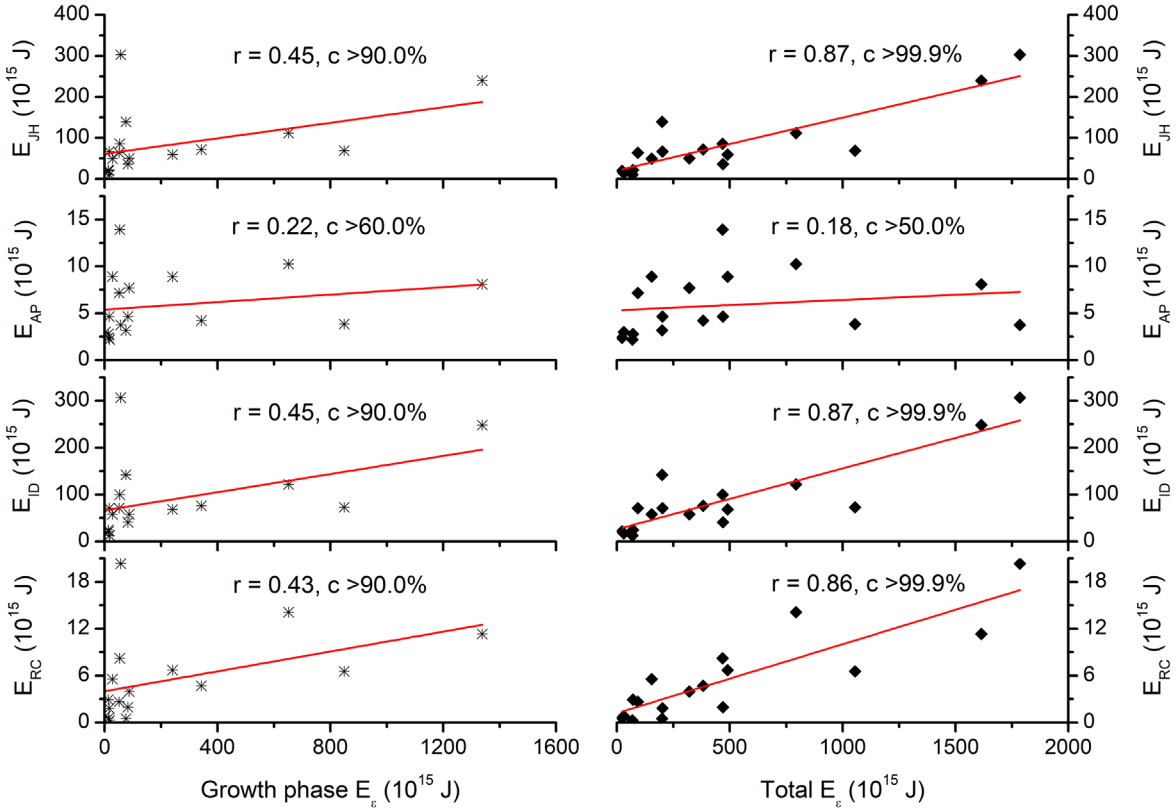

Figure 5. Variations of the energy dissipation through JH E_{JH}, AP E_{AP}, total ionospheric dissipation E_{ID}, and dissipation into the RC E_{RC} with the solar wind energy input during the substorm growth phases (left) and during the entire SSS intervals (right). Linear regression lines (red) and corresponding correlation coefficients (r) and confidence levels (c) are shown in each panel.

In agreement with the previous results of Hajra & Tsurutani (2018), it has been verified that the precursor energy during the substorm growth phase (during the 1.5 hr prior to the substorm expansion phase) in 9 (12) of the 17 shock-triggered SSS events was insufficient to account for the magnetospheric and ionospheric energy deposition through JH, AP, and RC energization. Thus, other sources of energy were considered, to be able to explain the large energy expended during the long-duration and extreme-intensity SSS events. It was shown in Figures 1 and 3 that for those two SSS events, the interplanetary shock compressed the preexisting southward IMFs (Tsurutani et al. 1988), leading to an abrupt increase in the solar wind energy input into the magnetosphere and ionosphere (as measured by the Akasofu ε parameter). As has been shown, this additional energy input was sufficient to supplement the 1.5 hr precursor energy in powering the entire magnetospheric and ionospheric energy dissipation during the expansion and recovery phases of the SSS events.

A solar wind energy input mechanism other than magnetic reconnection is solar wind ram energy. This was briefly discussed in the introductory section and was mentioned by Hajra & Tsurutani (2018) as a possible additional energy source. What is solar wind ram energy and how is it manifested in magnetospheric/ionospheric energy dissipation? Solar wind ram energy is the kinetic energy that is associated with the streaming velocity of solar wind protons and ions. It is essentially given by $E \sim 1/2\, m_i V_i^2$, associated with the streaming protons and Helium ions. The energy goes into the form of magnetospheric magnetic field compression, and consequential JH and the generation of Alfvén waves (Haerendel 1994). The Alfvén waves may propagate down the magnetic field lines and through Landau damping, accelerating the existing plasma to kiloelectronvolt energies. Dayside magnetospheric compression also causes preexisting magnetospheric energetic electrons and ions to be energized in $T_\perp$ (betatron acceleration), which then leads to temperature anisotropy instabilities (Kennel & Petschek 1966). The growth of both electron (chorus) and ion (EMIC) plasma waves leads to both electron and ion pitch-angle scattering and a diffuse aurora in the dayside ionosphere (Zhou & Tsurutani 1999; Tsurutani et al. 2001). The dayside auroras are not particularly intense, nor do they last long (~10–15 minutes). Thus, one expects the solar wind ram energy to occur only at the beginning of the SSS event, just at the release of the precursor stored energy. This amount of ram energy and the release of the precursor stored energy are apparently sufficient for only modest-intensity shock-triggered substorms.

Another possible energy source mentioned earlier in this paper is viscous interaction (Axford & Hines 1961; Tsurutani & Thorne 1982) between the solar wind and the magnetospheric flanks. However, Tsurutani & Gonzalez (1995) and Du et al. (2008) have indicated that the efficiency of this process is quite low. Tsurutani & Gonzalez (1995) have indicated an efficiency of ~1 to 4×10^{-3}. This is low, considering the numbers that have been shown in the body of this paper.

If the IMF is directed southward upstream of the interplanetary shock, the shock will compress this southward component (Tsurutani et al. 1988) by essentially a factor of the shock magnetosonic M_{ms} number (Kennel et al. 1985). This leads to an intensification of the ε parameter and the solar wind energy input into the magnetospheric/ionospheric system through magnetic reconnection. The high intensities of the

southward IMFs are most likely the cause of the unusual large-amplitude SSS peak intensities. Also, because the interplanetary sheath B_s durations can be longer than several hours, continued energy is pumped into the magnetosphere, explaining the long durations of the shock-triggered SSS events. See also Zong et al. (2021) for the long-duration SSS events.

Ordinary lower-intensity substorms are caused by IMF B_z variations in interplanetary Alfvén waves convected by the solar wind (Tsurutani & Meng 1972; Tsurutani et al. 1990, 2006a). These can be in either the slow solar wind or in high-speed streams. However, the main point is that the IMF intensities are of the order of ∼5 to 10 nT, with the B_z component only being a fraction of that value. The ε parameter will be small, leading to lower-intensity and shorter-duration substorms.

An energy storage mechanism that has previously been discussed in the literature is the enormous energy in the tail magnetic fields. Here, there is enough energy for a dozen substorms (Tsurutani et al. 1984a, 1984b, 1984c). However, this energy has not been invoked in Zhou & Tsurutani (2001), Hajra & Tsurutani (2018), or this paper, because it has not been necessary. There seems to be more than sufficient energy available in the solar wind during the substorm growth phase together with the enhanced solar wind energy input in the interplanetary sheath phase. The results of this paper show that if one assumes that the ε parameter is indeed a good proxy for the solar wind energy input, all the necessary energy for SSS events is present.

It was noted that when the IMF Bz turns southward, starting the SSS growth phase, the growth phase starts immediately, without delay. So there is both direct energy input into the magnetosphere/ionosphere system and the ∼1.5 hr storage. It has previously been indicated that all intense (Dst <-100 nT) magnetic storms could be accounted for by southward IMFs (Echer et al. 2008). Gonzalez et al. (1989) indicated that the delays from the IMF southward B_z peaks to the Dst/SYM-H peaks were ∼1–2 hr, approximately the same duration as for substorm energy storage. Thus, it is possible that for substorms, SSSs, and magnetic storms, all the energy is directly injected from the solar wind (with additional storage of up to ∼1.5 hr). The stored magnetotail energy may not be needed in any of these dynamic processes.

5. Final Comments

It can be noted from the statistical study of Hajra et al. (2016) that there was a general lack of an association of the SSS intensity with the geomagnetic storm intensity. However, for the two SSS cases shown in the present work, the events occur simultaneously with the concurrent magnetic storms, the latter being indicated by the SYM-H indices. Yue et al. (2011, 2016) have indicated that oxygen ions are injected into the magnetosphere during shock-triggered substorms. Thus, for the two cases shown in this paper, the RC energy input of the SSS events is the source of the magnetic storm RC. This is consistent with the Akasofu (1964) idea that substorms comprise parts of (or all of) magnetic storms. However, it should be mentioned that different substorm–storm relationships exist. High-intensity long-duration continuous AE activity events (Tsurutani & Gonzalez 1987; Tsurutani et al. 2006a, 2006b; Hajra et al. 2013) are substorms and DP2 events (Nishida 1968) that do not cause magnetic storms. Also, magnetic storms that are caused by smoothly rotating interplanetary MC fields may not have concurrent substorms (Tsurutani et al. 2004). The substorm–magnetic storm relationship is a complex one, which is still not totally understood.

In Figures 2 and 4 of this paper, it is noted that the dayside JH is essentially equivalent to the nightside JH, in agreement with the idea of a global current system (and dissipation), originally mentioned by Nishida (1968). It has also been reported by Tsurutani et al. (2001) that plasma waves have been detected at all local times on auroral-zone magnetic field lines. These waves are most likely caused by the instabilities associated with field-aligned currents. It is unfortunate that this important feature of the solar wind–magnetospheric coupling mechanism was not recognized previously. Perhaps too much focus has previously been placed on auroral breakups and the brilliant midnight-sector auroras.

NASA and ESA International Sun-Earth Explorer scientists worked hard at understanding collisionless shocks (fast, intermediate, and slow) for many years. They documented most of their years-long efforts in two volumes of AGU books (Stone & Tsurutani 1985; Tsurutani & Stone 1985) and two dedicated volumes of JGR (1985). Although this was done a generation ago, all of the material is relevant to space plasma research today. We encourage readers who are interested in shock-related phenomena to read these books and papers. It is also relatively easy to distinguish between discontinuities and fast shocks using publicly available high–time resolution plasma and magnetic field data. Instructions are given in Tsurutani et al. (2011) as to how to conduct these calculations. We hope that, in the future, workers in the field will calculate the shock properties themselves and include that information in their publications.

Data sources: (1) the AE SML indices and the MLT-dependent symmetric RC indices data are obtained from the SuperMAG website (https://supermag.jhuapl.edu/); (2) the solar wind/interplanetary data are obtained from the NASA OMNI data center (https://omniweb.gsfc.nasa.gov/); (3) the RC index SYM-H are obtained from the World Data Center for Geomagnetism, Kyoto, Japan (http://wdc.kugi.kyoto-u.ac.jp/); and (4) the APs are obtained from the NOAA/TIROS satellite (https://www.ngdc.noaa.gov/stp/satellite/poes/dataaccess.html). The work of R.H. is funded by the Science and Engineering Research Board (SERB; grant No. SB/S2/RJN-080/2018), a statutory body of the Department of Science and Technology (DST), Government of India, through the Ramanujan Fellowship. The authors declare no real or perceived financial conflicts of interests. The authors declare no conflicts of interest with respect to the results of this paper. We would like to dedicate this paper to the late Y. Kamide, A. Nishida, and the late H. Alfvén, who all strongly focused on field-line currents throughout their scientific lifetimes. Without their constant emphases, insights into the global nature of JH found in this paper might have been missed.

ORCID iDs

Bruce T. Tsurutani https://orcid.org/0000-0002-0094-7224
Rajkumar Hajra https://orcid.org/0000-0003-0447-1531

References

Abraham-Shrauner, B. 1972, JGR, 77, 736
Akasofu, S.-I. 1964, P&SS, 12, 273
Akasofu, S.-I. 1981, SSRv, 28, 121

Akasofu, S.-I., & Chao, J. K. 1980, P&SS, 28, 381
Axford, W. I., & Hines, C. O. 1961, CaJPh, 39, 1433
Boudouridis, A., Zesta, E., Lyons, R., Anderson, P. C., & Lummerzheim, D. 2003, JGRA, 108, 8012
Brittnacher, M., Wilber, M., Fillingim, M., et al. 2000, AdSpR, 25, 1377
Burch, J. L. 1972, JGR, 77, 5629
Burton, R. K., McPherron, R. L., & Russell, C. T. 1975, JGRA, 80, 4204
Chapman, S., & Ferraro, V. C. A. 1931, TeMAE, 36, 77
Chua, D., Parks, G., Brittnacher, M., et al. 2001, JGR, 106, 5945
Despirak, I., Kleimenova, N., Gromova, L., et al. 2019a, in E3S Web Conf. 127, X Anniversary Int. Conf. Solar-Terrestrial Relations and Physics of Earthquake Precursors (Les Ulis: EDP Sciences), 01010
Despirak, I. V., Lyubchich, A. A., & Kleimenova, N. G. 2019b, Ge&Ae, 59, 170
Despirak, I. V., Kleimenova, N. G., Gromova, L. I., et al. 2020a, Ge&Ae, 60, 292
Despirak, I. V., Lubchich, A. A., & Kleimenova, N. G. 2020b, in Proc. 12th Workshop "Solar Influences on the Magnetosphere, Ionosphere, Atmosphere" *(Primorsko, Bulgaria)*, 53
Despirak, I. V., Lubchich, A. A., & Kleimenova, N. G. 2020c, in Physics of Auroral Phenomena, Proc. XLIII Annual Seminar, Apatity (Murmansk: Polar Geophysical Inst.), 7
Despirak, I. V., Kleimenova, N. G., Lubchich, A. A., et al. 2021, in Physics of Auroral Phenomena, Proc. XLIV Annual Seminar, Apatity (Murmansk: Polar Geophysical Inst.), 12
Du, A., Tsurutani, B. T., & Sun, W. 2008, JGR, 113, A10214
Echer, E., Gonzalez, W. D., & Tsurutani, B. T. 2008, GeoRL, 35, L06S03
Emery, B. A., Evans, D. S., Greer, M. S., et al. 2006, The Low Energy Auroral Electron and Ion Hemispheric Power after NOAA and DMSP Intersatellite Adjustments, NCAR Scientific and Tech. rep. 470 Center for Atmospheric Research
Foster, J. C., Holt, J. M., Musgrove, R. G., & Evans, D. S. 1986, GeoRL, 13, 656
Fuller-Rowell, T. J., & Evans, D. S. 1987, JGR, 92, 7606
Gjerloev, J. W. 2012, JGRA, 117, A09213
Gonzalez, W. D., Tsurutani, B. T., Gonzalez, A. L. C., et al. 1989, JGR, 94, 8835
Guo, J., Feng, X., Emery, B. A., et al. 2011, JGRA, 116, A05106
Guo, J., Feng, X., Emery, B. A., & Wang, Y. 2012, JGRA, 117, A07303
Haerendel, G. 1994, ApJS, 90, 765
Hajra, R. 2022a, SoPh, 297, 14
Hajra, R. 2022b, SpWea, 20, e2021SW002937
Hajra, R., Echer, E., Tsurutani, B. T., & Gonzalez, W. D. 2013, JGRA, 118, 5626
Hajra, R., & Tsurutani, B. T. 2018, ApJ, 858, 123
Hajra, R., Tsurutani, B. T., Echer, E., & Gonzalez, W. D. 2014, GeoRL, 41, 1876
Hajra, R., Tsurutani, B. T., Echer, E., Gonzalez, W. D., & Gjerloev, J. W. 2016, JGRA, 121, 7805
Hajra, R., Tsurutani, B. T., & Lakhina, G. S. 2020, ApJ, 899, 3
Heppner, J. P. 1955, JGR, 60, 29
Hugoniot, H. 1887, Journal de l'École Polytechnique, 57, 3
Hugoniot, H. 1889, Journal de l'École Polytechnique, 58, 1
Kawasaki, K., Akasofu, S.-I., Yasuhara, F., & Meng, C.-I. 1971, JGR, 76, 6781
Kennel, C. F., Edmiston, J. P., & Hada, T. 1985, in Collisionless Shocks in the Heliosphere: A Tutorial Review, ed. R. G. Stone & B. T. Tsurutani (Washington, DC: AGU), 1
Kennel, C. F., & Petschek, H. E. 1966, JGR, 71, 1
Knipp, D. J., Tobiska, W. K., & Emery, M. A. 2004, SoPh, 224, 495
Kokubun, S., McPherron, R. L., & Russell, C. T. 1977, JGR, 82, 74
Liou, K., Newell, P. T., Meng, C.-I., Wu, C.-C., & Lepping, R. P. 2004, JGRA, 109, A06306
Ma, X.-H., Zong, Q.-G., & Liu, Y. 2019, JGRA, 124, 3210
Ma, J., Gao, X., Chen, H., et al. 2022, JGRA, 127, e2022JA030502
McPherron, R. L. 1970, JGR, 75, 5592
Monreal-MacMahon, R., & Gonzalez, W. D. 1997, JGR, 102, 14199
Newell, P. T., & Gjerloev, J. W. 2011, JGRA, 116, A12211
Nishida, A. 1968, JGR, 73, 5549
Oliveira, D. M., Weygand, J. M., Zesta, E., et al. 2021, SpWea, 19, e2021SW002933
Perreault, P., & Akasofu, S. I. 1978, GeoJI, 54, 547
Rankine, W. J. M. 1870, RSPT, 160, 277
Remya, B., Tsurutani, B. T., Reddy, R. V., Lakhina, G. S., & Hajra, R. 2015, JGRA, 120, 7536
Rostoker, G., Akasofu, S.-I., Foster, J., et al. 1980, JGR, 85, 1663
Schieldge, J. P., & Siscoe, G. L. 1970, JATP, 32, 1819
Shue, J. H., & Chao, J. K. 2013, JGRA, 118, 3017
Shue, J.-H., & Kamide, Y. 2001, GeoRL, 28, 2181
Shue, J.-H., Kamide, Y., & Newell, P. T. 2005, GeoRL, 32, L14112
Shue, J.-H., Kamide, Y., & Gjerloev, J. W. 2009, AnGeo, 27, 113
Smith, E. J. 1985, in Collisionless Shocks in the Heliosphere: Reviews of Current Research, ed. B. T. Tsurutani & R. G. Stone (Washington, DC: AGU)
Stone, R. G., & Tsurutani, B. T. 1985, Collisionless Shocks in the Heliosphere: A Tutorial Review, Geophys. Monogr. Ser., Vol. 4 (Washington DC: AGU), 34
Torr, M. R., Torr, D. G., Zukic, M., et al. 1995, SSRv, 71, 329
Tsurutani, B. T., & Meng, C. I. 1972, JGR, 77, 2964
Tsurutani, B. T., & Thorne, R. M. 1982, GeoRL, 9, 1247
Tsurutani, B. T., & Lin, R. P. 1985, JGRA, 90, 1
Tsurutani, B. T., & Gonzalez, W. D. 1987, P&SS, 35, 405
Tsurutani, B. T., Jones, D. E., Slavin, J. A., Sibeck, D. G., & Smith, E. J. 1984a, GeoRL, 11, 1062
Tsurutani, B. T., Jones, D. E., & Sibeck, D. G. 1984b, GeoRL, 11, 1066
Tsurutani, B. T., Slavin, J. A., Smith, E. J., Okida, R., & Jones, D. E. 1984c, GeoRL, 11, 1
Tsurutani, B. T., & Stone, R. G. 1985, Collisionless Shocks in the Heliosphere, Reviews of Current Research, Geophys. Monogr. Ser., Vol. 35 (Washington, DC: AGU), 35
Tsurutani, B. T., Gonzalez, W. D., Tang, F., Akasofu, S. I., & Smith, E. J. 1988, JGR, 93, 8519
Tsurutani, B. T., Gould, T., Goldstein, B. E., Gonzalez, W. D., & Sugiura, M. 1990, JGR, 95, 2241
Tsurutani, B. T., & Gonzalez, W. D. 1995, GeoRL, 22, 663
Tsurutani, B. T., & Lakhina, G. S. 1997, RvGeo, 35, 491
Tsurutani, B., Zhou, X. Y., Vasyliunas, V., et al. 2001, SGeo, 22, 101
Tsurutani, B. T., & Zhou, X.-Y. 2003, AdSpR, 31, 1063
Tsurutani, B. T., Gonzalez, W. D., Zhou, X.-Y., Lepping, R. P., & Bothmer, V. 2004, JASTP, 66, 147
Tsurutani, B. T., McPherron, R., Gonzalez, W. D., et al. 2006a, Recurrent Magnetic Storms: Corotating Solar Wind Streams, Geophys. Monogr. Ser., Vol. 167 (Washington, DC: AGU)
Tsurutani, B. T., Gonzalez, W. D., Gonzalez, A. L. C., et al. 2006b, JGRA, 111, A07S01
Tsurutani, B. T., Lakhina, G. S., Verkhoglyadova, O. P., et al. 2011, JASTP, 73, 5
Tsurutani, B. T., Hajra, R., Echer, E., & Gjerloev, J. W. 2015, AnGeo, 33, 519
Tsurutani, B. T., Hajra, R., Tanimori, T., et al. 2016, JGRA, 121, 10130
Tsurutani, B. T., Park, S. A., Falkowski, B. J., et al. 2019, JGRA, 124, 10063
Tsurutani, B. T., & Hajra, R. 2021, JSWSC, 11, 23
Turner, N. E., Baker, D. N., Pulkkinen, T. I., et al. 2001, JGRA, 106, 19149
Turner, N. E., Mitchell, E. J., Knipp, D. J., & Emery, B. A. 2006, in Recurrent Magnetic Storms: Corotating Solar Wind Streams, Geophys. Monogr. Ser., Vol. 167, ed. B. Tsurutani (Washington, DC: AGU), 113
Turner, N. E., Cramer, W. D., Earles, S. K., & Emery, B. A. 2009, JASTP, 71, 1023
Verkhoglyadova, O., Meng, X., Mannucci, A. J., et al. 2016, JSWSC, 6, A20
Yokoyama, N., & Kamide, Y. 1997, JGR, 102, 14215
Yue, C., Zong, Q. G., Zhang, H., et al. 2010, JGRA, 115, A00I05
Yue, C., Zong, Q., Wang, Y., et al. 2011, JGR, 116, A11206
Yue, C., Li, W., Nishimura, Y., et al. 2016, JGRA, 121, 6430
Yue, C., Chen, L., Bortnik, J., et al. 2017, JGRA, 122, 10047
Zesta, E., Singer, H. J., Lummerzheim, D., et al. 2000, in Geophys. Monogr. 118, Magnetospheric Current Systems, ed. S. Ohtani et al. (Washington, DC: AGU), 217
Zhou, X., & Tsurutani, B. T. 1999, GeoRL, 26, 1097
Zhou, X. Y., & Tsurutani, B. T. 2001, JGR, 106, 18957
Zhou, X.-Y., Strangeway, R. J., Anderson, P. C., et al. 2003, JGR, 108, 8019
Zhou, X. Y., & Tsurutani, B. T. 2004, JASTP, 63, 153
Zong, Q. G., Yue, C., & Fu, S. Y. 2021, SSRv, 217, 33